Earthquakes and Structures, *Vol. 10, No. 5 (2016) 1067-1087*
DOI: http://dx.doi.org/10.12989/eas.2016.10.5.1067

Design of a decoupled PID controller via MOCS for seismic control of smart structures

Sadegh Etedali*[1], Saeed Tavakoli[2a] and Mohammad Reza Sohrabi[3b]

[1]*Department of Civil Engineering, Birjand University of Technology, P.O. Box 97175-569, Birjand, Iran*
[2]*Faculty of Electrical and Computer Engineering, University of Sistan and Baluchestan, Zahedan, Iran*
[3]*Department of Civil Engineering, University of Sistan and Baluchestan, Zahedan, Iran*

(Received June 4, 2015, Revised March 16, 2016, Accepted April 3, 2016)

Abstract. In this paper, a decoupled proportional-integral-derivative (PID) control approach for seismic control of smart structures is presented. First, the state space equation of a structure is transformed into modal coordinates and parameters of the modal PID control are separately designed in a reduced modal space. Then, the feedback gain matrix of the controller is obtained based on the contribution of modal responses to the structural responses. The performance of the controller is investigated to adjust control force of piezoelectric friction dampers (PFDs) in a benchmark base isolated building. In order to tune the modal feedback gain of the controller, a suitable trade-off among the conflicting objectives, i.e., the reduction of maximum modal base displacement and the maximum modal floor acceleration of the smart base isolated structure, as well as the maximum modal control force, is created using a multi-objective cuckoo search (MOCS) algorithm. In terms of reduction of maximum base displacement and story acceleration, numerical simulations show that the proposed method performs better than other reported controllers in the literature. Moreover, simulation results show that the PFDs are able to efficiently dissipate the input excitation energy and reduce the damage energy of the structure. Overall, the proposed control strategy provides a simple strategy to tune the control forces and reduces the number of sensors of the control system to the number of controlled stories.

Keywords: seismic control; smart base isolated structures; piezoelectric friction dampers; multi-objective cuckoo search; PID controller

1. Introduction

Seismic isolation of structures and bridges is a method to reduce or eliminate the potential damages caused by dynamic loads such as earthquakes and strong winds (Naeim and Kelly 1999). However, recent studies on the performance of isolated structures have shown that isolation bearings experience very large displacements during near-field earthquakes (Jangid and Kelly 2001, Shen *et al*. 2004, Etedali and Sohrabi 2016). In order to enhance the performance of base-

*Corresponding author, Assistant Professor, E-mail: etedali@birjandut.ac.ir
[a]Associate Professor, E-mail: tavakoli@ece.usb.ac.ir
[b]Associate Professor, E-mail: sohrabi@hamoon.usb.ac.ir

http://www.techno-press.com/journals/eas&subpage=7 ISSN: 2092-7614 (Print), 2092-7622 (Online)

isolated structures against near-field earthquakes, passive, active and semi-active control devices have been suggested (Etedali *et al*. 2013a). Passive friction dampers are widely used as energy dissipation systems to reduce the base displacement of isolated structures under dynamic loads (Colajanni and Papia 1997, Gaul and Lenz 1997, Gaul and Nitsche 2001, Mualla and Belev 2002). These systems are not capable of adequately coping with variations in excitation loads; therefore, their performance is limited. However, passive friction dampers cannot adjust the slip force in real time. When the contact force is too large, the damper will not dissipate energy for weak and moderate earthquakes since it may not slide. On the other hand, when the contact force is reduced, the damper will have small energy dissipation capacity under strong earthquakes due to its small sliding friction force. Therefore, it is favorable to have a controllable contact force to provide the required amount of energy dissipation for various levels of earthquakes. Piezoelectric friction dampers (PFDs), as semi-active devices, are used for energy dissipation in structures. They can effectively suppress structural vibrations. Several experimental and theoretical studies have been conducted on these dampers in recent years. Chen and Chen (2000) offered a PFD embedded between the floor of a structure and its supporting bracket. Morita *et al*. (2001) proposed a base-isolated system equipped with PFDs. Li *et al*. (2004) presented a new design of PFD composed of piezoelectric actuators and an existing slot bolted connector. Chen and Chen (2004a) suggested a viscous and Reid friction (VRF) control strategy in which the control force was computed as a function of displacement and velocity of the damper. Also, they proposed a semi-active control algorithm to adjust the contact force of a PFD system applied to a 20-story steel structure (Chen and Chen 2004b). Using acceleration response as the feedback signal, Xu and Chen (2008) presented a modified VRF control strategy with a Kalman filter. To improve the performance of seismic isolation systems subjected to near-fault earthquakes, Lu and Lin (2009) proposed a semi-active isolation system equipped with PFD called a piezoelectric seismic isolation system (PSIS). Lu *et al*. (2010) developed a simple fuzzy controller for adjusting the friction force of PFDs in the PSIS. They showed that the proposed controller was very effective in suppressing the isolator displacement and story acceleration of the isolated system, simultaneously. In order to regulate the contact force of PFDs in an isolated structure, Ozbulut and Hurlebaus (2010) proposed two fuzzy logic controllers. Etedali *et al*. (2013a) developed optimal PD/PID controllers for seismic control of a benchmark isolated structure equipped with PFDs.

Because of its remarkable effectiveness and simplicity of implementation, PID controllers are known as the most popular industrial controllers. Although significant developments have been made in advanced control theory, most industrial controllers are still PID (Tavakoli *et al*. 2006). PID controllers are widely used in industrial control systems; however, few studies have been carried out on the use of them for seismic control of buildings (Guclu and Yazici 2007, Guclu and Yazici 2009, Etedali *et al*. 2013a). Considering a multiple-input multiple-output (MIMO) control system, the cross coupling of the plant channels makes it difficult to design each loop independently. In other words, adjusting controller parameters of one loop affects the performance of other loops (Tavakoli 2005). In structural control, the equation of motion of a structure is a set of N simultaneous differential equations, which are coupled by the off-diagonal terms in damping and stiffness matrices. This issue makes it difficult to design a MIMO PID controller.

This research work studies a simple approach for implementation of PID controllers in seismic-excited buildings. This strategy is a combination of PID controller with modal controller. At the first phase of this approach, the state space equation of a structure is transformed into modal coordinates. In the second phase, the parameters of the modal PID controller are determined in a reduced modal space. Then, according to the contribution of modal responses to the structural

responses, the feedback gain matrix is obtained. The proposed control strategy is employed to control variable friction dampers in a benchmark smart base isolation building. Although the base isolated structures have appropriate performance in far-field earthquakes, near-field earthquakes with long duration pulses result in very large displacements at the isolation level.

An effective control algorithm for seismic control of base-isolated structures should provide a good performance under various seismic excitations. In addition, sudden changes in the damper friction force of variable friction dampers can result in a high-frequency response. Due to such changes, the friction dampers tend to cause a large acceleration. To tune the modal feedback gain of the controller, a good trade-off among the conflicted objectives, namely the reduction of maximum modal base displacement, maximum modal floor acceleration of the smart base isolated structure, as well as maximum modal control force, should be made using the MOCS. Finally, the performance of the proposed controllers is compared with those resulted from other reported controllers for seven pairs of earthquakes.

The paper is organized as follows. The optimization procedure using the MOCS is explained in Section 2. The procedure of PID control design for seismic control of structures is explained in Section 3. In section 4, a decoupled PID controller is proposed for seismic control of structures. In section 5, numerical studies are carried out for a benchmark base-isolated structure equipped with PFDs. Simulation results are discussed in section 6. At the end, the concluding remarks are drawn.

2. Multi-objective cuckoo search

Metaheuristic algorithms are able to solve optimization problems without the need for a continuous and differentiable function. Furthermore, they are able to handle complex optimization problems and take into account the nonlinearities of the problems. Metaheuristic methods such as genetic algorithm (GA), particle swarm optimization (PSO), artificial bee colony algorithm (ABC), simulated annealing (SA) and harmony search (HS) have been applied to solve optimization engineering problems. Recently, a new metaheuristic search algorithm, called cuckoo search (CS), has been developed to solve optimization problems. This algorithm was introduced by Yang and Deb (2009). Two important features in the CS make this algorithm superior to many other metaheuristic algorithms. First, it applies Lévy flights, which are far more efficient than simple random walks. Lévy flight has infinite mean and variance. Therefore, it can explore search space better than standard Gaussian process and is useful to larger moves for a global search where the new moves can cover much more extensive regions. Second, the CS restores a balance between local search and global search exploration. The population size n, switching probability p_a, step-size α and Lévy flights exponent β are some configurable parameters of the CS. Compared with other algorithms, it has fewer algorithm-dependent parameters. Apart from the population size, switching probability is the main parameter of the CS. Other parameters such as Lévy flights exponent and step-size can be set as constants without affecting much on the performance of the algorithm. In contrast with α and β that have constant values 0.1 and 1.5 for most problems, p_a and n are variable and have great effects on the algorithm performance. Switching probability provides a balance between the local and global optimization. By increasing p_a, the probability for global optimization is reduced and vice versa (Yang and Deb 2009, Rajabioun 2011, Valian *et al*. 2013). Committed to the principles related to the single objective CS, Yang and Deb presented a MOCS for optimization problems with conflicting objectives. The following idealized rules are used in the MOCS (Yang and Deb 2013).

• Each cuckoo lays K eggs at a time, and dumps them in a randomly chosen nest. Egg k presents the solution to the K-th objective. This rule can be converted into a randomization process, so that a new solution can be randomly generated either by a random walk or by a Lévy flight. At the same time, a localized random permutation is performed over the solutions, which can be considered as a form of crossover. There can be K solutions for each nest.

• The best nests with a high quality of eggs (solutions) will carry over to the next generations. This rule is similar to elitism so that the best solutions are passed to the next generation. Such a selection of the best solutions helps the algorithm to ensure it converges properly.

• Each nest will be abandoned with a probability $p_a \in [0,1]$ and a new nest with K eggs will be built according to the similarities/differences of the eggs. In order to generate diversity, some random mixing can be used. This rule can be seen as a mutation so that the worst solutions are discarded at a certain probability and new solutions are generated, according to the similarity of the solutions to the other solutions.

Multi-objective optimization algorithms provide multiple optimal solutions, which form the so-called Pareto-optimal front. The Pareto-optimal front indicates the nature of the trade-off between the conflict objective functions. In order to obtain a good approximation for the Pareto front, a diverse range of solutions should be generated using efficient techniques. In the MOCS, a good diversity of the solutions is ensured by Lévy flights. To solve multi-objective problems associated with structural engineering, designers may be interested in a set of possible solutions, which provide alternative structural designs, instead of a single solution. This advantage provides the possibility to choose the best solution from among the presented solutions. In other words, the designer can select a possible solution that better fits with the designer's preferences.

3. PID control design for seismic control of structures

Considering the form of PID controller, its transfer function in the s domain, $K_{PID}(s)$, is given by Eq. (1), where k_C, τ_i and τ_d are proportional gain, integral time and differential time, respectively. Also, the PID control force in time domain, $u_{PID}(t)$, is determined using Eq. (2)

$$K_{PID}(s) = k_c\left(1 + \frac{1}{\tau_i s} + \tau_d s\right) \tag{1}$$

$$u_{PID}(t) = k_c\left[e(t) + \frac{1}{\tau_i}\int_0^t e(t)dt + \tau_d \frac{de(t)}{dt}\right] \tag{2}$$

where parameter t is the duration of the occurrence of an earthquake. Furthermore, $e(t)=y_{ref}(t)-y(t)$ is the error signal, which $y_{ref}(t)$ and $y(t)$ denote the reference input and the plant output, respectively. In structural control, it can be assumed that $y_{ref}(t)=0$, therefore $e(t)=-y(t)$. When the velocity of a story is feedback, the control force vector of the structure, $\mathbf{u}(t)$, can be expressed as

$$\mathbf{u}(t) = \mathbf{G}_c \mathbf{W}_c(t) \tag{3}$$

in which $\mathbf{G}_c$ refer to $n_c \times 3n_c$ feedback gain matrix and $\mathbf{W}_c(t)$ is a $3n_c \times 1$ feedback vector of the controller. Also, n_c represents the number of actuators, i.e., the number of controlled stories. $\mathbf{G}_c$ and $\mathbf{W}_c(t)$ are given by

$$\begin{aligned} \boldsymbol{G}_C &= \left[\boldsymbol{G}_{I_C} \quad \boldsymbol{G}_{P_C} \quad \boldsymbol{G}_{D_C}\right] \\ \boldsymbol{w}_C(t) &= [\boldsymbol{x}_C(t) \quad \dot{\boldsymbol{x}}_C(t) \quad \ddot{\boldsymbol{x}}_C(t)]^T \end{aligned} \tag{4}$$

where $\mathbf{G}_{I_C}$, $\mathbf{G}_{P_C}$ and $\mathbf{G}_{D_C}$ are $n_c \times n_c$ matrices. Moreover, $\mathbf{x_c}(t)$, $\dot{\mathbf{x}}_\mathbf{c}(t)$ and $\ddot{\mathbf{x}}_\mathbf{c}(t)$ refer to $n_c \times 1$ displacement, velocity and acceleration vectors of the controlled stories, respectively.

4. Decoupled PID control approach for seismic control of structures

In this section, a modal PID control design approach is proposed for seismic control of structures. This 2-phase hybrid control strategy combines the PID control design with control methods based on the modal space.

4.1 Phase 1

Considering an n-degree-of-freedom linear smart structure subjected to ground acceleration, $\ddot{x}_g(t)$, the equation of motion can be written as

$$\mathbf{M}\ddot{\mathbf{x}}(t) + \mathbf{C}\dot{\mathbf{x}}(t) + \mathbf{K}\mathbf{x}(t) = -\mathbf{M}\mathbf{r}\ddot{x}_g(t) + \mathbf{D}\mathbf{u}(t) \tag{5}$$

where $\boldsymbol{M}$, $\mathbf{C}$ and $\mathbf{K}$ are $n \times n$ mass, damping and stiffness matrices, respectively. $\mathbf{x}(t)$, $\dot{\mathbf{x}}(t)$ and $\ddot{\mathbf{x}}(t)$ refer to $n \times 1$ displacement, velocity and acceleration vectors, respectively. Also, $\mathbf{r}=[1,1,\ldots,1]^\mathbf{T}$ is an $n \times 1$ vector representing the seismic influence vector. Moreover, $\mathbf{D}$ is an $n \times n_c$ location matrix of control forces. Furthermore, $\mathbf{u}(t)$ represents an $n_c \times 1$ control force vector, where n_c is the number of actuators. There is a set of n simultaneous differential equations in Eq. (5), which are coupled by the off-diagonal terms in the mass and stiffness matrices. In the modal space, theses equations are transformed into a set of n independent normal coordinate equations. In order to obtain the state space equation in the modal space, the coordinate transformation is defined as

$$\mathbf{x}(t) = \mathbf{\Phi}\mathbf{y}(t) \tag{6}$$

where $\mathbf{y}(t)=[y_1(t),\ y_2(t),\ldots,y_n(t)]^T$ is the modal displacement vector and $\mathbf{\Phi}$ is an $n \times n$ orthonormalized mode shape matrix relative to the mass matrix. By substituting Eq. (6) in Eq. (5) and considering the term $\mathbf{\Phi}^T\mathbf{M}\mathbf{r}\ddot{x}_g(t)$ as the load disturbance, which must be applied to the structure, Eq. (5) can be written in the state space as follows

$$\begin{bmatrix} \dot{\mathbf{y}}(t) \\ \ddot{\mathbf{y}}(t) \end{bmatrix} = \begin{bmatrix} \mathbf{0} & \mathbf{I} \\ -\mathbf{\Omega}^2 & -\mathbf{C}_m \end{bmatrix} \begin{bmatrix} \mathbf{y}(t) \\ \dot{\mathbf{y}}(t) \end{bmatrix} + \begin{bmatrix} \mathbf{0} \\ \mathbf{I} \end{bmatrix} \mathbf{u}_m(t) \tag{7}$$

where $\mathbf{\Omega} = diag(\omega_1, \omega_2, \ldots, \omega_n)$ and $\mathbf{C}_m = diag(2\xi_1\omega_1, 2\xi_2\omega_2, \ldots, 2\xi_n\omega_n)$. Parameters ω_i and ξ_i are the natural frequency and modal damping ratio of the i-th mode. Also, $\mathbf{u}_m(t)$ is an $n \times 1$ modal control force vector, given by Eq. (8)

$$\mathbf{u}_m(t) = \mathbf{\Phi}^T\mathbf{D}\mathbf{u}(t) \tag{8}$$

The lower order modes of a structure subjected to seismic excitations usually provide the greatest contribution to the structural responses. Thus, it is reasonable to truncate analysis when the number of modes is sufficient. In other words, a control system can be designed based on the reduced modal space. By considering only n_{mc} ($n_{mc}<n$) modal equations from Eq. (7), Eq. (8) can be rewritten as

$$\mathbf{u}_{mc}(t) = \mathbf{\Phi}_{mc}^{T}\mathbf{D}\mathbf{u}(t) \tag{9}$$

where $\mathbf{\Phi}_{mc}$ is an $n\times n_{mc}$ matrix of the selected n_{mc} shape modes and $\mathbf{u}_{mc}$ is an $n_{mc}\times 1$ modal control force vector of the selected n_{mc} modes. In addition, the modal control force vector for the first n_{mc} modes of the structures, $\mathbf{u}_{mc}(t)$, can be expressed by

$$\mathbf{u}_{mc}(t) = \mathbf{G}_{mc}\mathbf{W}_{mc}(t) \tag{10}$$

where $\mathbf{G}_{mc}$ is an $n_{mc}\times 3n_{mc}$ modal feedback gain matrix and $\mathbf{W}_{mc}(t)$ is an $3n_{mc}\times 1$ modal feedback vector of the controller for the selected n_{mc} modes.

4.2. Phase 2

The transfer function of the PID controller in the i-th mode, $k_{mi}(s)$, can be defined as

$$k_{mi}(s) = k_{c_{mi}}\left(1+\frac{1}{\tau_{i_{mi}}s}+\tau_{d_{mi}}s\right) \tag{11}$$

where $k_{c_{mi}}, \tau_{i_{mi}}$ and $\tau_{d_{mi}}$ are proportional gain, integral time and differential time in the i- th mode of structure. Also, the PID control force in the i-th mode, $u_{mi}(t)$, can be given by

$$u_{mi}(t) = \mathbf{G}_{mi}\mathbf{W}_{mi}(t) \tag{12}$$

where $\mathbf{G}_{mi}$ is a 1×3 modal feedback gain vector and $\mathbf{W}_{mi}(t)$ is a 3×1 modal feedback vector of the controller in the i-th mode. These vectors can be obtained from the following equations

$$\begin{aligned}\mathbf{G}_{mi} &= k_{c_{mi}}\left[\frac{1}{\tau_{i_{mi}}} \quad 1 \quad \tau_{d_{mi}}\right] = \left[\mathbf{G}_{I_{mi}} \quad \mathbf{G}_{P_{mi}} \quad \mathbf{G}_{D_{mi}}\right]\\ \mathbf{w}_{mi}(t) &= \left[y_{mi}(t) \quad \dot{y}_{mi}(t) \quad \ddot{y}_{mi}(t)\right]^{T}\end{aligned} \tag{13}$$

Also, $y_{mi}(t)$, $\dot{y}_{mi}(t)$ and $\ddot{y}_{mi}(t)$ refer to the displacement, velocity and acceleration of structure in the i-th mode, respectively. By obtaining parameters of the PID controller in each mode, $\mathbf{G}_{mc}$ and $\mathbf{W}_{mc}(t)$ are given by

$$\begin{aligned}\mathbf{G}_{mc} &= \left[\mathbf{G}_{I_{mc}} \quad \mathbf{G}_{P_{mc}} \quad \mathbf{G}_{D_{mc}}\right]\\ \mathbf{w}_{mc}(t) &= \left[\mathbf{y}_{mc}(t) \quad \dot{\mathbf{y}}_{mc}(t) \quad \ddot{\mathbf{y}}_{mc}(t)\right]^{T}\end{aligned} \tag{14}$$

where $\mathbf{y}_{mc}(t)$, $\dot{\mathbf{y}}_{mc}(t)$ and $\ddot{\mathbf{y}}_{mc}(t)$ refer to $n_{mc}\times 1$ modal displacement, modal velocity and modal acceleration vectors of the selected n_{mc} modes, respectively. Furthermore, $\mathbf{G}_{I_{mc}}$, $\mathbf{G}_{P_{mc}}$ and $\mathbf{G}_{D_{mc}}$ are $n_{mc}\times n_{mc}$ matrices given by the following equations

$$\begin{aligned}\mathbf{G}_{I_{mc}} &= diag\,(G_{I_1}, G_{I_2}, ..., G_{I_{n_{mc}}})\\ \mathbf{G}_{P_{mc}} &= diag\,(G_{P_1}, G_{P_2}, ..., G_{P_{n_{mc}}})\\ \mathbf{G}_{D_{mc}} &= diag\,(G_{D_1}, G_{D_2}, ..., G_{D_{n_{mc}}})\end{aligned} \tag{15}$$

Using the relationship between $\mathbf{W}_{mc}(t)$ and $\mathbf{W}_c(t)$ and some algebraic efforts, the feedback gain matrix is obtained as follows (Etedali *et al*. 2013b)

$$\mathbf{G}_C = \begin{cases} \mathbf{E}^{-1}\mathbf{G}_{mc}\boldsymbol{\Psi}^{-1} & if \;\; n_{mc} = n_c \\ (\mathbf{E}^T\mathbf{E})^{-1}\mathbf{E}^T\mathbf{G}_{mc}\boldsymbol{\Psi}^T(\boldsymbol{\Psi}\boldsymbol{\Psi}^T)^{-1} & if \;\; n_{mc} > n_c \\ \mathbf{E}^T(\mathbf{E}\mathbf{E}^T)^{-1}\mathbf{G}_{mc}(\boldsymbol{\Psi}^T\boldsymbol{\Psi})^{-1}\boldsymbol{\Psi}^T & if \;\; n_{mc} < n_c \end{cases} \tag{16}$$

In Eq. (16), $\boldsymbol{\Psi}$ is a $3n_c \times 3n_{mc}$ matrix defined as

$$\boldsymbol{\Psi} = \begin{bmatrix} \boldsymbol{\varphi} & \mathbf{0} & \mathbf{0} \\ \mathbf{0} & \boldsymbol{\varphi} & \mathbf{0} \\ \mathbf{0} & \mathbf{0} & \boldsymbol{\varphi} \end{bmatrix} \tag{17}$$

where $\boldsymbol{\varphi}$ is an $n_c \times n_{mc}$ matrix obtained from removing the rows corresponding to the uncontrolled stories of the matrix $\boldsymbol{\Phi}_{mc}$. Also, $\mathbf{E} = \boldsymbol{\Phi}_{mc}^T\mathbf{D}$ is the modal participation matrix.

5. Numerical study

In order to evaluate the performance of the proposed controller in reducing the structural responses under earthquake loads, a five-story benchmark base-isolated building studied by Johnson *et al*. (1998) is considered. This structure has also been studied by Li and Ou (2006), Nagarajaiah and Narasimhan (2007), Ozbulut and Hurlebaus (2010), Ozbulut *et al*. (2011) and Etedali *et al*. (2013a). The structural mass of each story is equal to 5897 kg. From down to up, the damping coefficients for the five stories are 67, 58, 57, 50, and 38 kNs/m, respectively. Also, the corresponding stiffness coefficients are 33732, 29093, 28621, 24954, and 19059 kN/m, respectively. In case of having no isolator, the fundamental period and the damping ratio of the structure in the first mode are 0.3 second and 0.02, respectively. The isolation system, which consists of low-damping rubber bearings, assumed to have a linear force deformation behavior with a viscous damping. The total mass, damping coefficient and stiffness of the rubber bearings are 6800 kg, 7.48 kNs/m and 231.5 kN/m, respectively. The base isolated structure has a period of 2.5 seconds and a damping ratio of 0.04 in its fundamental mode. In order to improve the performance of the base-isolated building against different earthquakes, PFDs, with a total force capacity of 16.8 KN, are installed on the base of the structure. The experimental and analytical studies on the PFD have been carried out by Lu and Lin (2009). The schematic of the components of the PFD are shown in Fig. 1.

When this damper is subjected to an earthquake excitation, the relative motion between the friction bar and friction pad will generate a sliding force, which can be controlled by piezoelectric actuators. A piezoelectric actuator is embedded in the PFD to generate a vertical (contact)

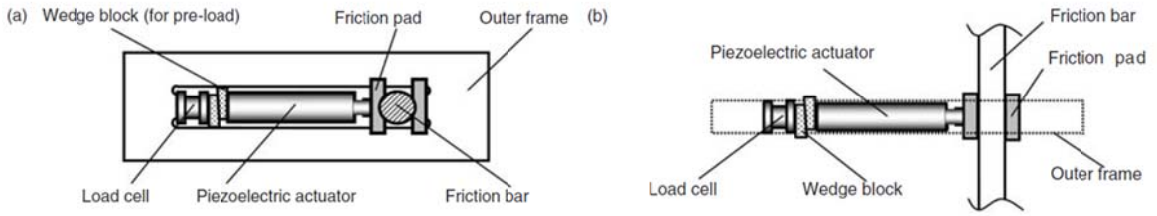

Fig. 1. The components of the PFD: (a) side view, (b) top view (Lu and Lin 2009)

controllable force. The vertical force in the PFD can be controlled by changing the input voltage of the piezoelectric actuator. A pair of wedge blocks is used to pre-compress the piezoelectric actuator. Also, a load cell is embedded in the PFD to measure the vertical force (Lu and Lin 2009, Lu *et al*. 2010). The contact force of the damper is given by

$$N(t) = N_0 + C_{PZ}V(t) \tag{18}$$

where $N(t)$ is the total vertical contact force, N_0 is the pre-compressor force, C_{PZ} is the friction coefficient of the PFD and $V(t)$ is the applied voltage to the stack actuator. Therefore, the friction force of the semi-active damper is obtained from

$$u(t) = \mu_d N(t) Sgn(\dot{x}) \quad \text{if } \dot{x} \neq 0 \tag{19}$$

$$-\mu_d N(t) < u(t) < \mu_d N(t) \quad \text{if } \dot{x} = 0 \tag{20}$$

where μ_d is the friction coefficient of materials between the friction bar and friction pad. Also, $sgn(\dot{x})$ denotes the sign of the slip velocity of the damper.

When the structure is moving under an earthquake excitation, two phases, sticking and slipping phases, are possible for the friction damper. A combination of sticking and slipping phases completely describes the state of the friction force. In the slipping phase, the sliding velocity is non-zero and the friction force can be computed by Eq. (19). In the sticking phase, two friction plates are stuck together and, hence, the sliding velocity is equal to zero. Therefore, the sticking phase of base-isolated structures happens when the friction damper is located between the base story and the ground. For numerical analyses, the absolute value of the friction force in the sticking phase can be approximated as follows

$$\left|u(t)\right| = \left|k_b x_b(t) + m_t \ddot{x}_g(t)\right| \quad \text{when } \dot{x} = 0 \tag{21}$$

where k_b is the isolator stiffness, x_b is the relative displacement of base-isolators, m_t is the total mass of the structure and $\ddot{x}_g(t)$ is the ground acceleration (He *et al*. 2003). As long as the above condition applies, the two plates will remain in the stack mode during the sticking phase.

The control forces provided by linear feedback control laws are active control forces, which cannot be achieved by semi-active devices. The PFD in PSIS is basically a variable passive damper. It only produces a resistance force and its direction is always opposite to the slip velocity. Also, the desired control force can be realized when the damper is in the slipping phase. (Ng and Xu 2007). Therefore, the following criterion is used to adjust the desired control force, $N(t)$.

$$N(t) = \begin{cases} \dfrac{u_{Active}}{\mu} & \text{if } u_{Active}.\dot{x}_b < 0 \\ 0 & \text{if } u_{Active}.\dot{x}_b \geq 0 \end{cases} \tag{22}$$

where u_{Active} is the control force obtained from the linear feedback control and μ is coulomb friction coefficient. After determining the contact force, the actuator voltage $V(t)$, which is an online control law, can be directly determined by Eq. (23)

$$0 \leq V(t) = \frac{N(t) - N_o}{C_{PZ}} \leq V_{max} \tag{23}$$

The PFD parameters used in this study are identical to the parameters used in experimental studies by Lu and Lin (2009). The parameters N_{pre}, C_{PZ} and μ_{d} are equal to 1000 N, 1.10 N/V and 0.2, respectively. Also, the maximum actuator voltage is 1000 V.

The PID control design in a reduced modal space can be seen as an optimization problem. In seismic control of structures, acceptable structural responses and control force may be achieved by solving such an optimization problem. In the case of semi-active control of a base isolated building using PFDs, a sudden change in the friction force of PFDs can increases the floor acceleration of the superstructure. In addition, the large displacement of isolator in near-field earthquakes is a major challenge for designers. An optimal tuning of the controller should aim at reducing the isolation displacement without any increase in the acceleration response of the superstructure. Therefore, a MOCS algorithm is used to provide a good trade-off between these conflicting objectives in a reduced modal space. For this purpose, three objective functions are defined for the optimization problems in each mode. J_{1i} and J_{2i} are respectively the maximum modal base displacement and floor acceleration in the i-th mode of the controlled structure normalized by their corresponding values in the uncontrolled structure. The uncontrolled structure is a structure with no control force feedback and control tools. J_{3i} is defined as the modal control force normalized by the modal weight of structure in the i-th mode. Due to the limited capacity of the total control force of PFDs, it is assumed that the amount of J_{3i} is limited to 0.05. To reduce the structural responses for different earthquake excitations, the proposed control strategy must reject load disturbances well. The artificial ground acceleration is used to model the earthquakes. A band limited Gaussian white noise, made by filtering a Gaussian white noise, is produced to model the artificial ground acceleration. By considering several earthquakes, one well-known filter was introduced by Kanai (1961). The output of this filter simulates the earthquake. Nagarajaiah and Narasimhan (2006), introduced a modified form of Kanai-Tajimi filter according to Eq. (24)

$$F(s) = \frac{4\xi_g \omega_g S}{S^2 + 2\xi_g \omega_g S + \omega_g^2} \tag{24}$$

where ξ_g and ω_g are the ground damping and frequency, respectively. In this study, ξ_g=0.3 and ω_g=2π rad/s are used for numerical simulations.

By testing a different range of effective parameters of the CS, namely the population size and switching probability, we found that the best values of these parameters are n=20, p_a=0.25. In the design of the modal controller, the first three modes are selected for the control of the benchmark structure. Considering this structure subjected to the ground artificial acceleration, Fig. 2 shows the Pareto-optimal curve for the first three modes. This curve provides the possibility to choose an

appropriate solution from a set of non-dominated solutions. Each member of the Pareto-optimal curve represents a vector in the design space. Considering an appropriate solution provided by the MOCS for the first three modes, the PID controllers for the selected modes are as follows

$$k_{m1}(s) = 127.12(1 + \frac{1}{9.72s} + 0.02s) \tag{25}$$

$$k_{m2}(s) = 0.98(1 + \frac{1}{8.47s} + 0.00284s) \tag{26}$$

$$k_{m3}(s) = 0.02(1 + \frac{1}{3.17s} + 0.00692s) \tag{27}$$

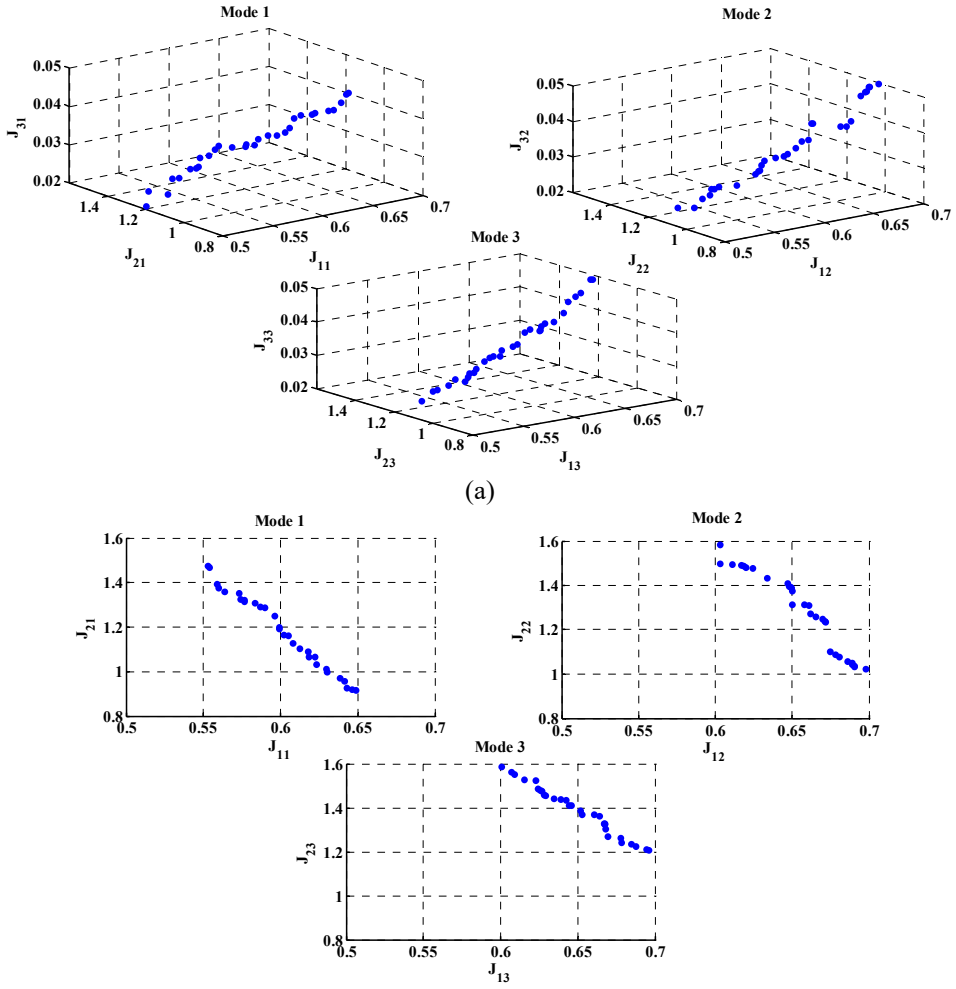

Fig. 2 the Pareto-optimal front diagrams for the first three modes: (a) perspective, (b) side view

It is remarkable that the values of the control gains in the first mode are larger than the corresponding values in other modes. In other words, participation of higher modes is less than that of fundamental mode of the structure. After determining the PID controller parameters in the controlled modes of the structure, the modal feedback gain matrix, $\mathbf{G}_{mc}$, is obtained from Eq. (14). Then, the feedback gain matrix of controller, $\mathbf{G}_c$, is obtained through substituting $\mathbf{G}_{mc}$ in Eq. (16).

6. Results and discussion

To evaluate the performance of the proposed control strategy and compare it with that of other reported techniques, a set of fault-parallel (FP) and fault-normal (FN) components of El Centro, Newhall, Sylmar, Rinaldi, Kobe, Chi-Chi, Erzinkan, considered by Narasimhan *et al*. (2006) in structural control of smart base isolated structures, are used. Simulation results and time history analyses of the base-isolated building are obtained using MATLAB/Simulink. The quantities of the maximum displacement of isolators, $x_{b,max}$, maximum inter-story drift, $d_{s,max}$, maximum absolute floor acceleration of superstructure, $\ddot{x}_{s,max}$, maximum damper force, $F_{d,max}$, maximum root mean squared of base displacement, $\sigma_{xb,max}$, and maximum root mean squared of floor acceleration of superstructure, $\sigma_{\ddot{x}s,max}$, are considered to evaluate the performance of the various control strategies. The maximum absolute floor acceleration of the superstructure and its RMS value are given by $\ddot{x}_{s,max}=\max(\ddot{x}_{1,max}, \ddot{x}_{2,max}, \ddot{x}_{3,max}, \ddot{x}_{4,max}, \ddot{x}_{5,max})$ and $\sigma_{\ddot{x}s,max}=\max(\sigma_{\ddot{x}1,max}, \sigma_{\ddot{x}2,max}, \sigma_{\ddot{x}3,max}, \sigma_{\ddot{x}4,max}, \sigma_{\ddot{x}5,max})$, where $\ddot{x}_{i,max}$ and $\sigma_{\ddot{x}i,max}$ (i=1,2,3,4,5) refer to the maximum absolute acceleration of the i-th floor and its RMS value.

The results are given in Tables 1 and 2. For comparison purposes, the results provided by the maximum passive operation of piezoelectric friction dampers; modified clipped-optimal controller, supervisory fuzzy logic controller (SVFLC), self-organizing fuzzy logic controller (SOFLC), and optimal PID controller are also listed in these tables. The results for the base-isolated building without any damper, i.e., uncontrolled structure, are also listed in these tables. Demanding the maximum voltage, the results show that the maximum passive operation of PFDs successfully reduces the maximum isolation displacement and the value of its RMS, in most earthquakes. However, this controller significantly increases the maximum floor acceleration for most of cases. In comparison with the uncontrolled structure, for example, the maximum passive operation of PFDs results in 73%, 80% and 38% increase in the peak story acceleration for the FN component of El Centro, Newhall and Kobe earthquakes, respectively. For the same earthquakes, the increase is as much as 131%, 135%, and 156% for the FP component, respectively. In comparison with the modified clipped optimal controller, the maximum passive operation performs better in reducing the maximum base displacement at the cost of increasing the maximum floor acceleration. When the PFDs are modulated by a clipped-optimal controller, there is an increase of 71%, 30% and 20% in the maximum floor accelerations compared to the uncontrolled cases for the FN component of El Centro, Newhall and Kobe earthquakes, respectively. The increase is as much as 80%, 59%, and 95% for the FP component of the same earthquakes, respectively. The results obtained from the SVFLC and SOFLC show that these methods successfully limit the increase in the peak floor acceleration for the same excitation cases, while at the same time satisfactorily reduce the maximum isolator deformations. Also, the performance of PID controller shows that it is able to reduce the displacement of the isolator for different earthquakes without losing the advantages of the isolation. Also, it is observed that the proposed control strategy is able to reduce the maximum base displacement and floor acceleration, simultaneously. When the performance of the proposed

control strategy is compared with those given by SVFLC and SOFLC, it can be seen that the proposed controller is more effective than these controller, especially in controlling the acceleration response of the base-isolated building. In comparison with other controllers, i.e., SVFLC, SOFLC and PID controller, the proposed controller performs better in reducing the maximum base displacement at the cost of a slight increase in the maximum floor acceleration, in most earthquakes. Considering the FP component of El Centro earthquake, for example, SVFLC, SOFLC and PID controller provide a reduction of 48%, 55% and 26% in the maximum base

Table 1 Maximum responses of the base isolated building subjected to FP component of earthquakes

Earthquake	Control case	$x_{b,max}$ (cm)	$d_{s,max}$ (cm)	$\ddot{x}_{s,max}$ (m/s^2)	$F_{d,max}$ (KN)	$\sigma_{xb,max}$ (cm)	$\sigma_{\ddot{x}s,max}$ (m/s^2)
El Centro	Uncontrolled	20.36	0.13	1.86	-	0.08	0.52
	Maximum passive operation	4.89	0.13	4.30	16.80	0.01	0.83
	Modified clipped optimal controller	10.38	0.10	3.35	16.80	0.03	0.66
	SVFLC	10.59	0.09	2.48	13.25	0.03	0.48
	SOFLC	9.16	0.08	3.02	15.55	0.02	0.51
	Optimal PID	15.15	0.10	1.47	6.49	0.05	0.34
	Proposed controller	5.09	0.10	1.56	13.51	0.02	0.56
Newhall	Uncontrolled	33.65	0.31	3.65	-	0.11	0.85
	Maximum passive operation	10.09	0.31	8.58	16.80	0.02	0.81
	Modified clipped optimal controller	14.80	0.22	5.81	16.80	0.04	0.64
	SVFLC	12.79	0.20	4.60	16.80	0.04	0.50
	SOFLC	12.11	0.21	4.89	16.80	0.03	0.50
	Optimal PID	19.90	0.23	3.28	12.61	0.06	0.57
	Proposed controller	17.16	0.22	3.29	13.82	0.03	0.59
Sylmar	Uncontrolled	62.40	0.36	4.64	-	0.23	1.52
	Maximum passive operation	31.20	0.24	3.57	16.80	0.07	0.76
	Modified clipped optimal controller	44.92	0.28	4.17	16.80	0.12	0.91
	SVFLC	40.56	0.27	3.80	16.80	0.10	0.76
	SOFLC	37.44	0.26	3.80	16.80	0.09	0.71
	Optimal PID	38.82	0.24	3.43	16.80	0.10	0.74
	Proposed controller	31.20	0.23	3.43	16.80	0.07	0.61
Rinaldi	Uncontrolled	71.98	0.41	5.55	-	0.26	1.68
	Maximum passive operation	37.43	0.26	4.00	16.80	0.09	0.84
	Modified clipped optimal controller	54.71	0.33	5.39	16.80	0.14	1.03
	SVFLC	48.95	0.30	4.33	15.99	0.12	0.89
	SOFLC	46.07	0.29	4.27	16.80	0.11	0.86
	Optimal PID	44.37	0.27	3.47	16.80	0.11	0.81
	Proposed controller	36.71	0.25	3.44	16.13	0.08	0.72

Table 1 Continued

Earthquake	Control case	$x_{b,max}$ (cm)	$d_{s,max}$ (cm)	$\ddot{x}_{s,max}$ (m/s^2)	$F_{d,max}$ (KN)	$\sigma_{xb,max}$ (cm)	$\sigma_{\ddot{x}s,max}$ (m/s^2)
Kobe	Uncontrolled	28.15	0.23	3.02	-	0.08	0.58
	Maximum passive operation	13.80	0.22	7.73	16.80	0.03	0.98
	Modified clipped optimal controller	18.30	0.26	5.89	16.80	0.05	0.91
	SVFLC	16.61	0.19	4.05	16.80	0.04	0.60
	SOFLC	16.61	0.19	4.20	16.80	0.04	0.61
	Optimal PID	18.32	0.17	2.40	14.60	0.05	0.46
	Proposed controller	14.08	0.19	2.32	16.80	0.03	0.49
Chichi	Uncontrolled	59.51	0.33	3.88	-	0.13	0.87
	Maximum passive operation	32.73	0.23	3.14	16.75	0.06	0.59
	Modified clipped optimal controller	38.68	0.24	3.57	16.76	0.08	0.62
	SVFLC	37.49	0.23	2.83	15.55	0.08	0.56
	SOFLC	36.30	0.23	2.91	16.53	0.07	0.58
	Optimal PID	39.59	0.23	2.69	16.80	0.08	0.55
	Proposed controller	33.92	0.23	2. 76	16.29	0.06	0.49
Erzincan	Uncontrolled	44.96	0.27	3.53	-	0.19	1.25
	Maximum passive operation	26.53	0.21	5.40	16.80	0.07	0.77
	Modified clipped optimal controller	42.01	0.33	4.61	16.80	0.15	1.16
	SVFLC	39.32	0.32	3.85	14.45	0.13	1.00
	SOFLC	38.24	0.32	4.12	16.80	0.12	1.00
	Optimal PID	40.44	0.31	3.67	16.20	0.16	1.08
	Proposed controller	26.53	0.20	3.71	16.80	0.07	0.91

displacement in comparison with the uncontrolled structure, while this reduction is 75% for the proposed controller. Considering the FP component of Kobe earthquake, the reduction is 41%, 41%, 35% and 50% for SVFLC, SOFLC, PID controller and proposed controller, respectively. Compared to the uncontrolled cases for the FP component of El-Centro and Kobe earthquakes, SVFLC leads to an increase of 33% and 34% in the maximum floor acceleration. Similarly, an increase of 62% and 39% is obtained for SOFLC. However, the PID and proposed controller manage to provide a reduction of 21% and 16% for the FP component of El Centro earthquake and 21% and 23% for the FP component of Kobe earthquake in the maximum floor acceleration.

In addition, the results indicate that the proposed controller maintain acceptable responses in terms of the maximum inter-story drifts as well as the RMS values of the base displacement and floor acceleration.

For the proposed control approach, the time histories of the isolator displacement and top floor acceleration under the FP component of the El Centro and Sylmar, as far-field and near-field earthquakes, are illustrated in Figs. 3 and 4, respectively. The results of the uncontrolled structure are also shown in these figures. It is observed that the proposed controller effectively reduces the

Table 2 Maximum responses of the base isolated building subjected to FN component of earthquakes

Earthquake	Control case	$x_{b,max}$ (cm)	$d_{s,max}$ (cm)	$\ddot{x}_{s,max}$ (m/s^2)	$F_{d,max}$ (KN)	$\sigma_{xb,max}$ (cm)	$\sigma_{\ddot{x}s,max}$ (m/s^2)
El Centro	Uncontrolled	24.14	0.14	2.17	-	0.07	0.49
	Maximum passive operation	6.76	0.10	3.75	16.80	0.01	0.79
	Modified clipped optimal controller	12.31	0.11	3.71	16.80	0.02	0.62
	SVFLC	11.34	0.10	2.71	12.46	0.02	0.48
	SOFLC	9.65	0.10	2.60	15.07	0.02	0.52
	Optimal PID	16.59	0.11	2.00	8.06	0.04	0.33
	Proposed controller	7.24	0.10	2.12	13.45	0.02	0.48
Newhall	Uncontrolled	37.04	0.38	5.07	-	0.10	0.77
	Maximum passive operation	27.41	0.38	9.13	16.80	0.06	1.08
	Modified clipped optimal controller	31.86	0.38	6.59	16.80	0.08	0.85
	SVFLC	30.75	0.37	5.73	16.80	0.07	0.80
	SOFLC	30.00	0.38	6.44	16.80	0.07	0.83
	Optimal PID	31.87	0.37	4.53	16.80	0.07	0.57
	Proposed controller	27.78	0.36	4.61	16.80	0.05	0.66
Sylmar	Uncontrolled	82.20	0.47	8.16	-	0.31	2.03
	Maximum passive operation	49.32	0.33	6.29	16.80	0.13	1.03
	Modified clipped optimal controller	60.01	0.37	7.26	16.80	0.20	1.34
	SVFLC	53.43	0.34	6.45	16.80	0.16	1.14
	SOFLC	52.61	0.35	6.94	16.80	0.15	1.03
	Optimal PID	50.16	0.31	7.71	16.80	0.14	0.99
	Proposed controller	50.14	0.33	7.75	14.84	0.13	0.97
Rinaldi	Uncontrolled	53.86	0.38	4.48	-	0.14	0.95
	Maximum passive operation	40.39	0.35	4.79	16.80	0.08	0.82
	Modified clipped optimal controller	45.24	0.35	4.70	16.80	0.09	0.85
	SVFLC	46.67	0.38	4.48	16.80	0.09	0.70
	SOFLC	42.34	0.35	3.96	14.14	0.08	0.64
	Optimal PID	41.39	0.35	3.97	16.07	0.08	0.63
	Proposed controller	39.85	0.33	4.13	16.80	0.07	0.69
Kobe	Uncontrolled	31.74	0.24	3.75	-	0.07	0.64
	Maximum passive operation	18.09	0.20	5.18	16.80	0.04	1.08
	Modified clipped optimal controller	24.76	0.21	4.50	16.80	0.05	0.92
	SVFLC	23.49	0.21	3.49	16.80	0.05	0.72
	SOFLC	22.85	0.21	3.94	16.80	0.05	0.76
	Optimal PID	15.97	0.12	1.98	13.24	0.03	0.29
	Proposed controller	20.22	0.22	2.15	16.30	0.04	0.53

Table 2 Continued

Earthquake	Control case	$x_{b,max}$ (cm)	$d_{s,max}$ (cm)	$\ddot{x}_{s,max}$ (m/s^2)	$F_{d,max}$ (KN)	$\sigma_{xb,max}$ (cm)	$\sigma_{\ddot{x}s,max}$ (m/s^2)
Chichi	Uncontrolled	123.77	0.70	8.07	-	0.29	1.84
	Maximum passive operation	73.03	0.45	5.49	16.80	0.14	1.01
	Modified clipped optimal controller	95.31	0.56	6.62	16.13	0.20	1.33
	SVFLC	76.74	0.46	5.65	15.21	0.15	1.05
	SOFLC	79.22	0.48	6.30	16.80	0.16	1.07
	Optimal PID	84.34	0.51	6.05	16.80	0.15	1.01
	Proposed controller	66.84	0.42	5.08	16.80	0.14	0.96
Erzincan	Uncontrolled	74.18	0.42	4.79	-	0.29	1.86
	Maximum passive operation	51.93	0.34	4.17	16.39	0.15	1.12
	Modified clipped optimal controller	59.35	0.36	4.60	15.96	0.19	1.31
	SVFLC	54.90	0.34	3.98	15.21	0.17	1.14
	SOFLC	53.41	0.33	4.12	16.18	0.15	1.07
	Optimal PID	51.87	0.31	3.61	16.80	0.15	1.04
	Proposed controller	52.43	0.34	3.56	16.39	0.15	1.04

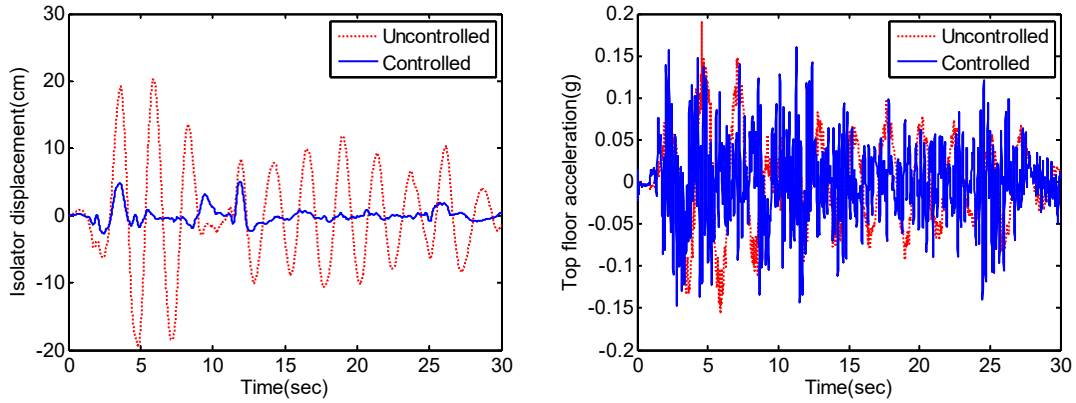

Fig. 3 Time histories of isolator displacement and top story acceleration of the uncontrolled and semi active controlled structure subjected to El Centro earthquake

base displacement of the isolated building in both far-field and near-field earthquakes. Also, it can be seen that this controller is even able to reduce the maximum top story acceleration of the isolated building in both earthquakes.

For the same earthquakes, the hysteresis loops of the isolators for the controlled structure are also compared with those of the uncontrolled building in Figs. 5 and 6. In these figures, the total shear force includes the total friction and restoring force in the elastomeric bearings and w is the weight of the structures. Also, the time history of the command voltage for the proposed control approach is shown in these figures. Considering the hysteresis loops of isolation systems, shown in these figures, it can be seen that PFDs increase the height and decrease the width of the hysteresist

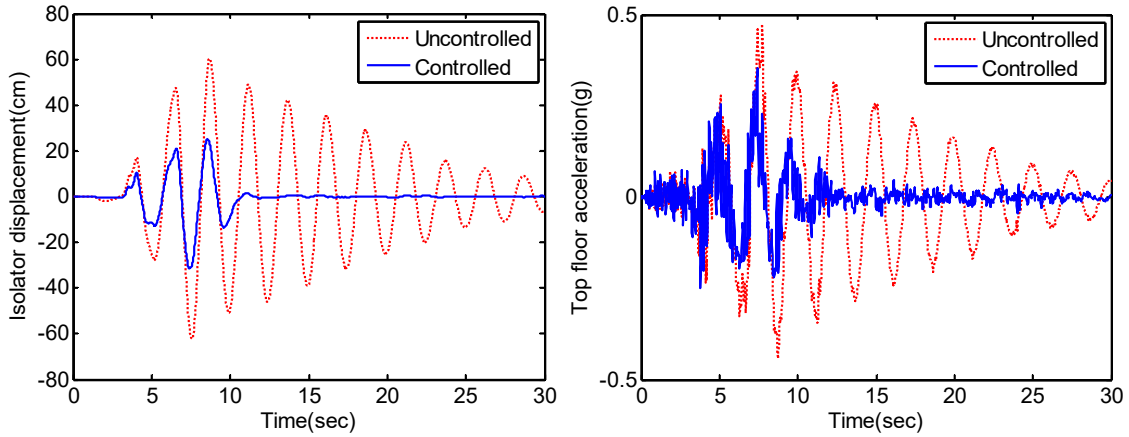

Fig. 4 Time histories of isolator displacement and top story acceleration of uncontrolled and semi active controlled structure subjected to Sylmar earthquake

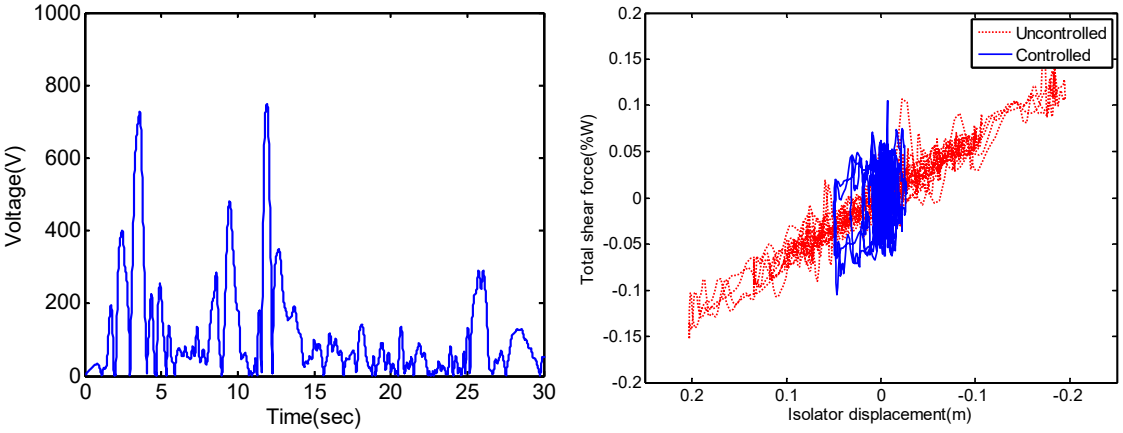

Fig. 5 Hysteresis loops of isolation systems and time history of the command voltage for the base-isolated building subjected to the El Centro earthquake

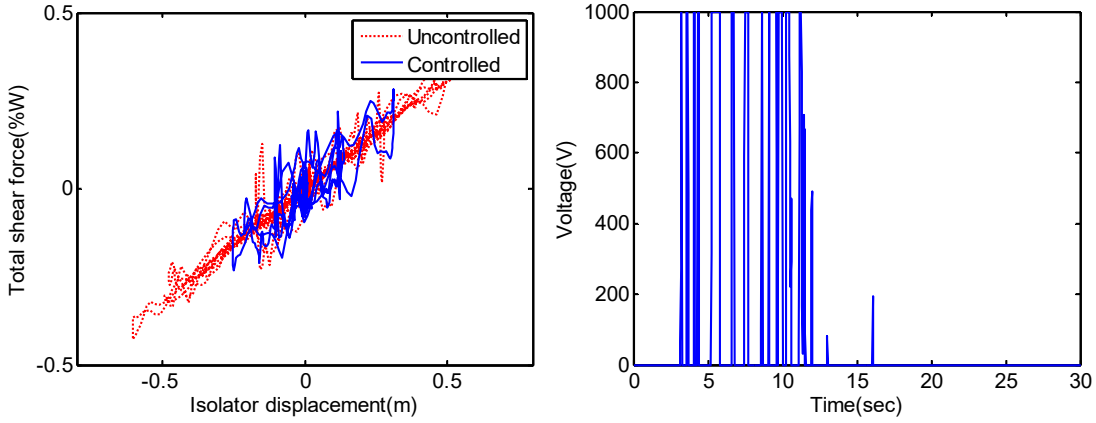

Fig. 6 Hysteresis loops of isolation systems and time history of the command voltage for the base-isolated building subjected to the Sylmar earthquake

loop when the proposed controller is applied to adjust its contact force. This implies that the PFDs decrease the displacement of the isolators, but maintain the same level of energy dissipation capacity for the isolation system by increasing the damping force. Considering the time history of the command voltage for the semi-active control, it can be concluded that the proposed controller requests a higher value of voltage in the near-filed earthquakes in comparison with the far-filed ones.

Vibration control of a structure subjected to an earthquake can be described as an energy transfer process. The energy balance equation of a linear base-isolated structure equipped with PFDs can be presented by Eq. (28)

$$E_K + E_D + E_S + E_{PFD} = E_I \tag{28}$$

where, E_K, E_D and E_S are the absolute kinetic, damping and elastic strain energies. Also, E_I and E_{PFD} denote the hysteretic energy provided by the PFDs and the absolute seismic input energy. Note that the sum of the kinetic energy and strain is known as the total energy of the system or the damage energy. For the FP component of El Centro and Sylmar earthquakes, Figs. 7 and 8

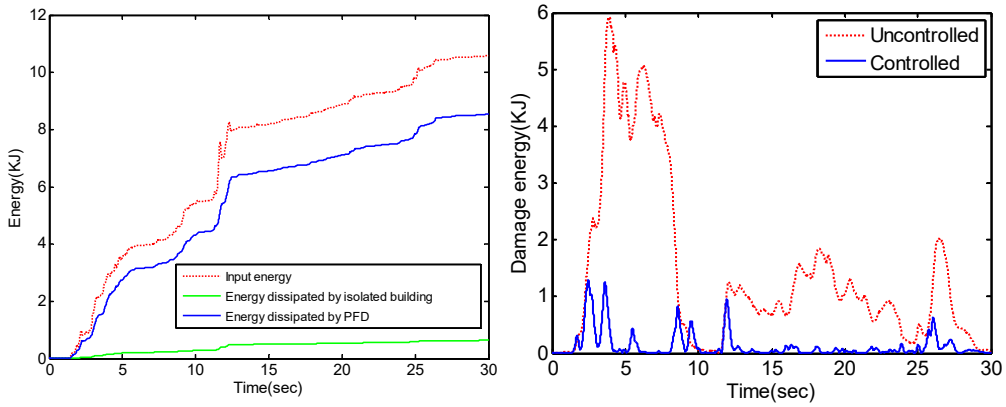

Fig. 7 Time histories of energy for the controlled base-isolated building and time histories of damage energy for uncontrolled and controlled base-isolated buildings subjected to El Centro earthquake

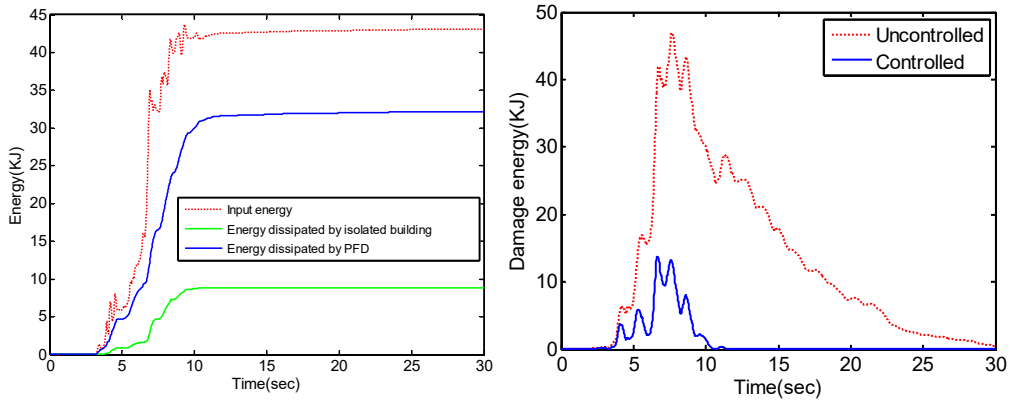

Fig. 8 Time histories of energy for the controlled base-isolated building and time histories of damage energy for uncontrolled and controlled base-isolated buildings subjected to Sylmar earthquake

respectively illustrate the time histories of the input energy, E_I, viscous damped energy of the building and isolators, E_D, and the energy dissipated by the PFD, E_{PFD}, for the controlled base-isolated building with the proposed controller. For the same excitations, time histories of the damage energy for both uncontrolled and controlled base-isolated buildings are also shown in these figures. Obviously, most of the input excitation energy is appropriately dissipated by the PFDs. Also, when the base-isolated building is subjected to El Centro earthquake, the damage energy of the controlled building using the proposed controller is reduced about 78% in comparison with the uncontrolled building without any damper. This reduction is about 71% for Sylmar earthquake.

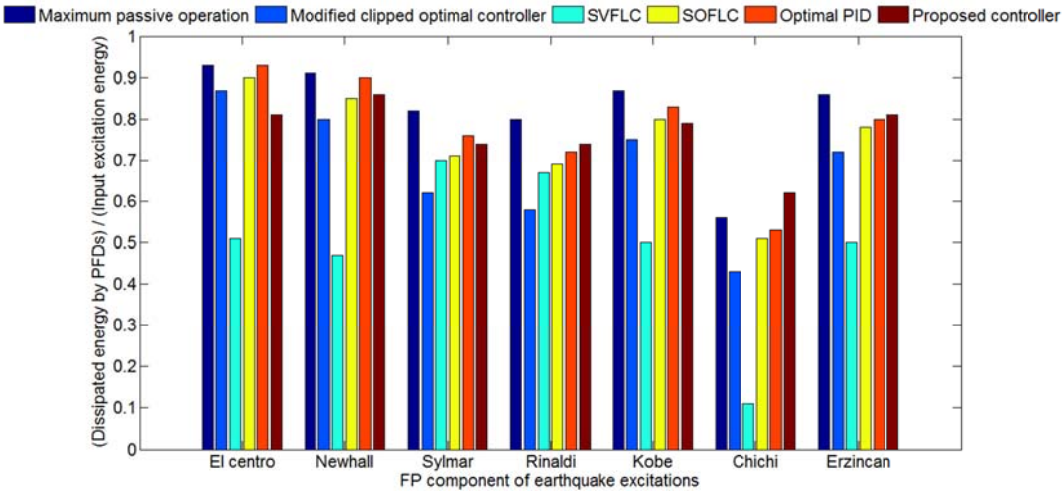

Fig. 9 The dissipated energy by PFDs normalized by the input excitation energy for FP component of earthquake excitations

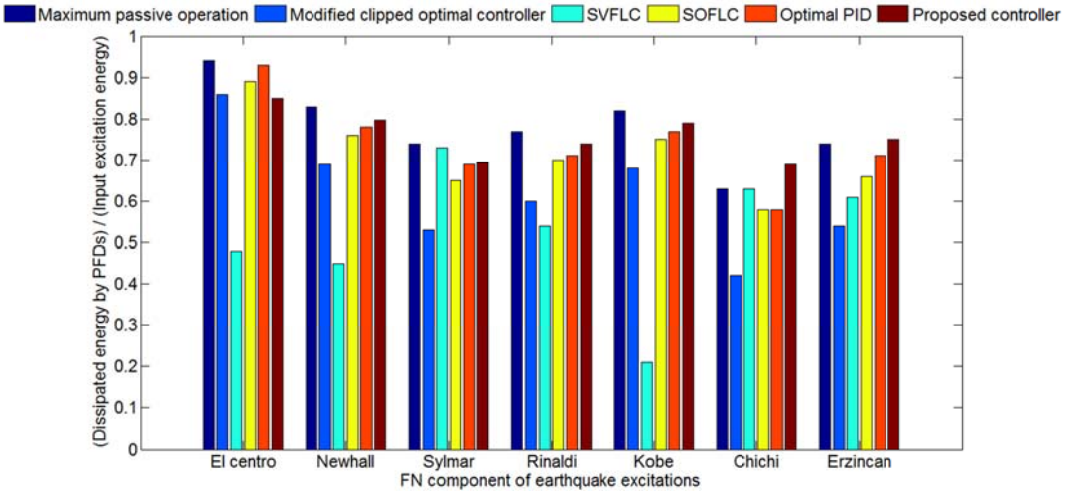

Fig. 10 The dissipated energy by PFDs normalized by the input excitation energy for FN component of earthquake excitations

In order to compare the performance of the proposed controller with that of other control approaches in terms of the dissipated energy by PFDs, Figs. 9 and 10 are illustrated. In these figures, the dissipated energy by PFDs is normalized by the input excitation energy. Considering the results obtained from Tables 1-2 and Figs. 9-10, it is found that the selected control strategy to adjust the contact force of PFDs plays a key role in the dissipation of input excitation energy and seismic performance of base isolated structures. Furthermore, it can be seen that the maximum passive operation of piezoelectric friction dampers performs better than other control strategies in terms of dissipation of input excitation energy. However, as shown in Tables 1 and 2, the performance of the controller in simultaneous reduction of the maximum base displacement and maximum acceleration of stories is not satisfactory. For most earthquakes, the proposed controller is able to dissipate the input excitation energy better than the modified clipped optimal controller, SVFLC, SOFLC and optimal PID controller. Moreover, according to the results shown in Tables 1 and 2, the proposed controller performs better than SVFLC, SOFLC and optimal PID controller in reducing the maximum base displacement at the cost of a slight increase in the maximum floor acceleration.

It should be noted that the displacement, velocity and acceleration of the controlled stories are required to adjust the control force by the proposed controller. In fact, the proposed controller needs to be equipped with only one sensor to measure the feedback signal of the controlled story. Also, two computational resources are required for each controlled story of the structure. For this benchmark building, the proposed controller has to be equipped with one sensor on the base story to measure its velocity and two computational resources to determine the displacement and acceleration of the base story. Because of the limitation in the number of required sensors for measuring state variables in large structures, the proposed control strategy has many advantages in terms of simplicity, reliability and cost in comparison with common modern control methods such as LQG and LQR.

7. Conclusions

In this paper, a modal-PID controller was presented for seismic control of structures. In the modal coordinates, n coupled equations of motion of an n-degree-of-freedom structure were transformed into a set of n decoupled equations. In the reduced modal space, the modal feedback gain of the controller was designed. Then, based on the contribution of the modal responses to the structural responses, the feedback gain matrix of the controller was obtained. The proposed controller was used for adjusting the contact force of piezoelectric friction dampers in a benchmark base isolated building. To create a balance between two important structural responses, i.e. the maximum base displacement and maximum floor acceleration, subject to a physical limitation on the maximum control force, the modal feedback gain of the controller was designed using an optimization procedure based on the MOCS. Fourteen components of earthquakes were taken into account to investigate the performance of the suggested controller. Also, the performance of the proposed controller was compared with that of the maximum passive operation of the friction dampers, modified clipped optimal controller, SVFLC, SOFLC and optimal PID controller. The simulation results showed that the proposed controller performed better than others control strategies in terms of simultaneous reduction of maximum base displacement and story acceleration during both near-field and far-field ground motions. Also, the results demonstrated that the proposed controller was able to significantly dissipate most of input seismic energy and reduce the damage energy of the building. One important advantage of the proposed control strategy was that it reduced the number of sensors of the

control system to the number of controlled stories. For the benchmark base isolated structure, the controller needed only one sensor to measuer the velocity of the base story and two computational resources to determine its displacement and acceleration in real time. In fact, the proposed control approach provided a simple control system with advantages in terms of simplicity, reliability and cost in comparison with the common modern control methods such as LQG and LQR.

References

Chen, G. and Chen, C. (2000), "Behavior of piezoelectric friction dampers under Dynamic loading", *Proceedings of the SPIE - Smart structures and materials*, **3988**, 54-63.

Chen, G. and Chen, C. (2004a), "Shaking table test of quarter-scale building model with piezoelectric friction dampers", *Struct. Contr. Hlth. Monit.*, **11**(4), 293-257.

Chen, G. and Chen, C. (2004b), "Semi active control of the 20-Story benchmark building with piezoelectric friction dampers", *J. Eng. Mech.*, **130**(4), 393-400.

Colajanni, P. and Papia, M. (1997), "Hysteretic characterization of friction-damped braced frames", *J. Struct. Eng.*, **123**(8), 1020-1028.

Etedali, S., Sohrabi, M.R. and Tavakoli, S. (2013a), "Optimal PD/PID control of smart base isolated buildings equipped with piezoelectric friction dampers", *Earthq. Eng. Eng. Vib.*, **12**(1), 39-54.

Etedali, S., Sohrabi, M.R. and Tavakoli, S. (2013b), "An independent robust modal PID control approach for seismic control of buildings", *J. Civ. Eng. Urban.*, **3**(5), 279-291.

Etedali, S. and Sohrabi, M.R. (2016), "A proposed approach to mitigate the torsional amplifications of asymmetric base-isolated buildings during earthquakes", *KSCE J. Civ. Eng.*, **20**(2), 768-776.

Gaul, L. and Lenz, J. (1997), "Nonlinear dynamics of structures assembled by bolted joints", *Acta Mechanica*, **125**(1), 169-181.

Gaul, L. and Nitsche, R. (2001), "The role of friction in mechanical joints", *Appl. Mech. Rev.*, **54**(2), 93-106.

Guclu, R. and Yazici, H. (2007), "Fuzzy-logic control of a non-linear structural system against earthquake induced vibration", *J. Vib. Contr.*, **13**(11), 1535-1551.

Guclu, R. and Yazici, H. (2009), "Seismic-vibration mitigation of a nonlinear structural System with an ATMD through a fuzzy PID controller", *Nonlinear Dyn.*, **58**(3), 553-564.

He, W.L., Agrawal, A.K. and Yang, J.N. (2003), "Novel semi active friction controller for linear structures against earthquakes", *J. Struct. Eng.*, **129**(7), 941-950.

Jangid, R.S. and Kelly, J.M. (2001), "Base isolation for near-fault motion", *Earthq. Eng. Struct. Dyn.*, **30**(5), 691-707.

Johnson, E.A., Ramallo, J.C., Spencer Jr, B.F. and Sain, M.K. (1998), "Intelligent base isolation systems", *Proceedings Second World Conference on Structural Control*, **1**, 367-376.

Kanai, K. (1961), "An empirical formula for the spectrum of strong earthquake motions", *Bull. Earthq. Res. Inst.*, **39**, 85-95.

Li, J., Li, H. and Song, G. (2004), "Semi-active vibration suppression using piezoelectric friction dampers based on sub-optimal bang-bang control laws", *3rd China-Japan-US Symposium on Structural Health Monitoring and Control*.

Li, H. and Ou, J. (2006), "A design approaches for semi-active and smart base-isolated buildings", *Struct. Contr. Hlth. Monit.*, **13**(2-3), 660-681.

Lu, L.Y., Lin, C.C., Lin, G.L. and Lin, C.Y. (2010), "Experiment and analysis of a fuzzy-controlled piezoelectric seismic isolation system", *J. Sound Vib.*, **329**(11), 1992-2014.

Lu, L.Y. and Lin, G.L. (2009), "A theoretical study on piezoelectric smart isolation system for seismic protection of equipment in near-fault areas", *J. Intel. Mater. Syst. Struct.*, **20**(2), 217-232.

Morita, K., Fujita, T., Ise, S., Kawaguchi, K., Kamada, T. and Fujitani, H. (2001), "Development and application of induced strain actuators for building Structures", *Proceedings of the SPIE-Smart structures and materials*, **4330**, 426-437.

Mualla, I.H. and Belev, B. (2002), "Performance of steel frames with a new friction damper device under earthquake excitation", *Eng. Struct.*, **24**(3), 365-371.
Naeim, F. and Kelly, J.M. (1999), *Design of Seismic Isolated Structures from Theory to Practice*, John Wiley & Sons, 2nd Edition.
Nagarajaiah, S. and Narasimhan, S. (2006), "Smart base-isolated benchmark building part II: phase I, sample controllers for linear and friction isolation", *Struct. Contr. Hlth. Monit.*, **13**(2-3), 589-604.
Nagarajaiah, S. and Narasimhan, S. (2007), "Seismic control of smart base isolated buildings with new semi active variable damper", *Earthq. Eng. Struct. Dyn.*, **36**(6), 729-749.
Narasimhan, S., Nagarajaiah, S., Johnson, E.A. and Gavin, H.P. (2006), "Smart base-isolated benchmark building part I: Problem definition", *Struct. Contr. Hlth. Monit.*, **13**(2-3), 573-588.
Ng, C.L. and XU, Y.L. (2007), "Semi-active control of a building complex with variable friction dampers", *Eng. Struct.*, **29**(6), 1209-1225.
Ozbulut, O.E., Bitaraf, M. and Hurlebaus, S. (2011), "Adaptive control of base-isolated structures against near-field earthquakes using variable friction dampers", *Eng. Struct.*, **33**(12), 3143-3154.
Ozbulut, O.E. and Hurlebaus, S. (2010), "Fuzzy control of piezoelectric friction dampers for seismic protection of smart base isolated buildings", *Bull. Earthq. Eng.*, **8**(6), 1435-1455.
Rajabioun, R. (2011), "Cuckoo optimization algorithm", *Appl.Soft Comput.*, **11**(8), 5508-5518.
Shen, J., Tsai, M.H., Chang, K.C. and Lee, G.C. (2004), "Performance of a seismically isolated bridge under near-fault earthquake ground motions", *J. Struct. Eng.*, **130**(6), 861-868.
Tavakoli, S. (2005), "Multivariable PID control with application to gas turbine engines", Ph.D. Dissertation. University of Sheffield, UK.
Tavakoli, S., Griffin, I. and Fleming, P.J. (2006), "Tuning of decentralized PI (PID) controllers for TITO processes", *Contr. Eng. Pract.*, **14**(9), 1069-1080.
Valian, E., Tavakoli, S., Mohanna, S. and Haghi, A. (2013), "Improved cuckoo search for reliability optimization problems", *Comput. Indust. Eng.*, **64**(1), 459-468.
Xu, Y.L, and Chen, B. (2008), "Integrated vibration control and health monitoring of building structures using semi-active friction dampers: Part I-methodology", *Eng. Struct.*, **30**(7), 1789-1801.
Yang, X.S. and Deb, S. (2009), "Cuckoo search via Lévy flights", *The World Congress on Nature & Biologically Inspired Computing (NaBIC)*, 210-214.
Yang, X.S. and Deb, S. (2013), "Multi objective cuckoo search for design optimization", *Comput. Operat. Res.*, **40**(6), 1616-1624.

KT